The Astrophysical Journal Letters, 971:L5 (8pp), 2024 August 10 https://doi.org/10.3847/2041-8213/ad5b4c

On the Association of GW190425 with Its Potential Electromagnetic Counterpart FRB 20190425A

Ignacio Magaña Hernandez[1], Virginia d'Emilio[2,3], Soichiro Morisaki[4], Mohit Bhardwaj[1], and Antonella Palmese[1]
[1] McWilliams Center for Cosmology, Department of Physics, Carnegie Mellon University, Pittsburgh, PA 15213, USA; imhernan@andrew.cmu.edu
[2] Cardiff University, Cardiff CF24 3AA, UK; demiliov@caltech.edu
[3] California Institute of Technology, Pasadena, CA 91125, USA
[4] Institute for Cosmic Ray Research, The University of Tokyo, 5-1-5 Kashiwanoha, Kashiwa, Chiba 277-8582, Japan
Received 2024 April 17; revised 2024 June 11; accepted 2024 June 24; published 2024 July 31

Abstract

Recent work by Moroianu et al. has suggested that the binary neutron star (BNS) merger GW190425 might have a potential fast radio burst (FRB) counterpart association, FRB20190425A, at the 2.8σ level of confidence with a likely host galaxy association, namely UGC10667. The authors argue that the observations are consistent with a long-lived hypermassive neutron star (HMNS) that formed promptly after the BNS merger and was stable for approximately 2.5 hr before promptly collapsing into a black hole. Recently, Bhardwaj et al. conclusively associated FRB20190425A with UGC10667, potentially providing a direct host galaxy candidate for GW190425. In this work, we examine the multimessenger association based on the spacetime localization overlaps between GW190425 and the FRB host galaxy UGC10667 and find that the odds for a coincident association are $\mathcal{O}(5)$. We validate this estimate by using a Gaussian process density estimator. Assuming that the association is indeed real, we then perform Bayesian parameter estimation on GW190425 assuming that the BNS event took place in UGC10667. We find that the viewing angle of GW190425 excludes an on-axis system at $p(\theta_v > 30^\circ) \approx 99.99\%$, highly favoring an off-axis system similar to GRB 170817A. We also find a slightly higher source frame total mass for the binary, namely, $m_{\rm total} = 3.42^{+0.34}_{-0.11} M_\odot$, leading to an increase in the probability of prompt collapse into a black hole and therefore disfavors the long-lived HMNS formation scenario. Given our findings, we conclude that the association between GW190425 and FRB20190425A is disfavoured by current state-of-the-art gravitational-wave analyses.

Unified Astronomy Thesaurus concepts: Gravitational waves (678); Radio transient sources (2008)

1. Introduction

The first detection of gravitational waves by Advanced LIGO (Aasi et al. 2015) and Virgo (Acernese et al. 2014) from the merger of two neutron stars, GW170817, allowed for the first multimessenger studies using both gravitational-wave (GW) data and electromagnetic (EM) observations (Abbott et al. 2019). Following the binary neutron star (BNS) merger, a burst of short gamma-rays (sGRB) was detected by Fermi and INTEGRAL about 2 s after the GW emission (Abbott et al. 2017). As neutron star (NS) matter collided, a kilonova (KN) was produced and was eventually observed 11.4 hr after GW170817 was detected (Nicholl et al. 2017; Soares-Santos et al. 2017). This allowed for the unique identification of the host galaxy of GW170817, a relatively old and massive galaxy, namely NGC4993. Follow-up, radio observations determined a radio afterglow that was first observed around 100 days after GW170817 and that is still detectable to date (Balasubramanian et al. 2022).

The detection of GW170817 and its many EM counterparts, in particular, GRB 170817A allowed for the study of the statistical significance that both the GW and sGRB events originated from a common astrophysical source. Given the 2 second time delay between GW170817 and GRB 170817A as well as the typical Fermi sGRB detection rate, it was concluded that from timing considerations alone, the coincident (common source) hypothesis was favored by $\mathcal{O}(10^6)$ times more than a mere chance of random association. Further studies (see for example Piotrzkowski et al. 2022) used the small localization volume for GW170817 and its host galaxy, NGC4993, to study the statistical chance of spatial association. These studies arrived at similar conclusions; however, we note that the most stringent constraints were placed by the time delay between GW170817 and GRB 170817A. With such strong odds, it is believed that these two events and the follow-up EM observations were all due to the first detectable merger of NSs in both GWs and light.

During the first half of the LIGO-Virgo-KAGRA (LVK) third observing run (O3a; Abbott et al. 2024; Akutsu et al. 2021), GW190425, a second high-confidence detection of GWs from a BNS merger was discovered(Abbott et al. 2020b). The GWs were observed initially only by the LIGO Livingston observatory but Virgo was also functional at the time. The two detector network detection did not allow for precise sky localization and GW190425 was localized to around 10^5 deg^2 in the sky. The large sky localization region and the fact that this event happened at a distance of about 200 Mpc did not allow for the detection of any confidently associated electromagnetic counterparts in low latency.

Recent work by Moroianu et al. (2023) has found evidence at a 2.8σ level for the association between GW190425 and the fast radio burst FRB20190425A detected by the CHIME Collaboration about 2.5 hr after the BNS merger with a likely host galaxy association, namely UGC10667. Follow-up work by Panther et al. (2023) used the FRB20190425A sky localization region to first identify possible host galaxies for the transient. Using approximately a couple of orders of magnitude precise baseband localization of FRB20190425A, Bhardwaj et al. (2023b) robustly

associated UGC10667 as the host galaxy of FRB20190425A, with a probability of chance association of <0.1%. The most plausible host galaxy candidate, consistent with Moroianu et al. (2023), as well as the expected host galaxies for FRBs and the measured properties of FRB20190425A was found to be UGC10667 with a probability of chance association of <0.1% (Bhardwaj et al. 2023b).

However, we note that optical imaging 6 hr (3.5 hr) after GW190425 (FRB20190425A) of UGC10667 did not find any promising optical emission as well as follow-up observations around 1 day and after 2 weeks did not reveal any promising transients (Smartt et al. 2024). Additionally, Panther et al. (2023) performed follow-up Very Large Array observations of UGC10667 to see if a radio afterglow would be detectable. Assuming an on-axis viewing angle and a lack of detectable afterglow for the putative transients, Panther et al. (2023) argue that the merger had to likely be off-axis since an on-axis merger would give rise to a detectable afterglow.

Given the total mass for GW190425 was found to be $3.4^{+0.3}_{-0.1}\ M_{\odot}$, the LVK collaboration suggested that the two NSs most likely collapsed into a black hole promptly. This is consistent with our current constraints on the equation of state (EOS) for dense nuclear matter (Abbott et al. 2020a). Moroianu et al. (2023) and Zhang (2023), however, put forward a proposed scenario to suggest a mechanism for the potential FRB emission and to explain the delay of the merger. In order for the proposed NS to not collapse directly into a black hole, it is necessary to invoke a highly spinning remnant, as this might provide increased mass support, as well as a stiffer EOS and potentially an exotic compact object as one of the binary components, e.g., a quark star. The hypermassive NS would then survive the direct collapse for about 2.5 hr until it collapses into a black hole ejecting its magnetosphere in the process leading to the production of FRB20190425A.

In this work, we reexamine the association between GW190425 and FRB20190425A by considering spatial and temporal coincidence including the limited field of view of CHIME. We assume that UGC10667 is the host galaxy for both GW190425 and FRB20190425A in our posterior odds calculations. We then perform GW parameter estimation on GW190425 under the assumption that UGC10667 is indeed the host for both transients to have a direct measurement of the viewing angle to the BNS event as well as improved mass estimates.

2. GW190425 and FRB20190425A Association

To examine the association between the GW event GW190425 and its potential EM counterpart FRB20190425A, we follow the formalism in Ashton et al. (2018, 2021) to compute the posterior odds for a common source for the two transients. We compare two hypotheses: a common source C, in which the GW190425 postmerger remnant produces an FRB counterpart by ejecting its magnetosphere before collapsing onto a black hole (Moroianu et al. 2023); and a random coincidence hypothesis R, in which both events are entirely distinct.

The agreement between posterior distributions, under the common source hypothesis, is quantified by the posterior overlap integral. For a given set of parameters θ, the integral is defined as,

$$\mathcal{I}_{\theta} = \int \frac{p(\theta|d_{\rm GW}, C)p(\theta|d_{\rm EM}, C)}{\pi(\theta|C)} d\theta, \quad (1)$$

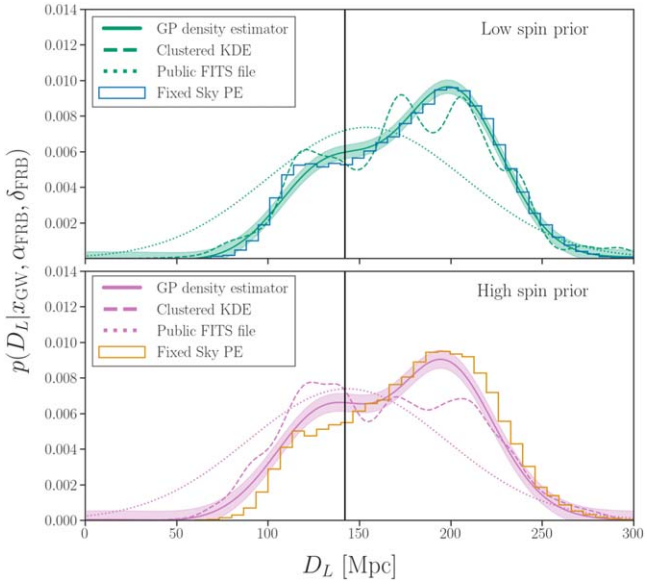

Figure 1. Posterior probability of the luminosity distance from GWTC-3 samples marginalized along the FRB line-of-sight (LOS; black line). The top panel shows low-spin results; the bottom panel shows high-spin results. The marginal posterior distribution is computed using localization `FITS` files (dotted line), a Clustered KDE (dashed line), and a GP density estimator (solid line). The shaded band shows the GP's 2σ uncertainty. The LOS PE samples obtained in this work are also shown here for comparison (as histograms).

where $p(\theta|d_{\rm GW}, C)$ is the parameter's posterior given the GW observation, $p(\theta|d_{\rm EM}, C)$ is the parameter's probability from EM, and $\pi(\theta|C)$ is the parameter's prior distribution.

Considering both spatial and temporal coincidences between the GW and FRB observations, as mathematically derived in Ashton et al. (2018; Equation (5)), the posterior odds between the two competing hypotheses can then be calculated as,

$$\mathcal{O}_{C/R} = \pi_{C/R}\mathcal{I}_{D_L,\Omega}\mathcal{I}_{t_c} \approx \pi_{C/R}\mathcal{I}_{D_L}\mathcal{I}_{\Omega}\mathcal{I}_{t_c}, \quad (2)$$

where $\mathcal{I}_{D_L,\Omega}$ is the overlap integral for the three-dimensional localization volumes between the two transients and $\mathcal{I}_{D_L}$ and $\mathcal{I}_{\Omega}$ are the overlap integrals for the approximately disjoint luminosity distance and sky localizations, respectively. The temporal overlap integral is given by $\mathcal{I}_{t_c}$ and $\pi_{C/R}$ is the ratio of probabilities for the two hypotheses based solely on prior information, e.g., the detection rates for the transients.

2.1. Spatial Overlap

To measure the posterior odds of GW190425 being associated with FRB20190425A we use the publicly available LVK posterior samples on the parameters of GW190425 (Abbott et al. 2020b, 2023; LVK Scientific Collaboration 2020a).

The joint posterior overlap integral $\mathcal{I}_{D_L,\Omega}$ requires interpolating the three-dimensional posterior density $p(D_L, \Omega|d_{\rm GW}, C)$. Since GW190425 was not a well-localized event, the density surface presents degenerate correlations and non-Gaussianities. To assess the goodness of the three-dimensional fit, we look at the one-dimensional slice of the interpolation and of the GWTC-3 samples over the FRB sky location, as shown in Figure 1. For comparison purposes, we compute the interpolation with `ligo.skymap`'s ClusteredKDE (Singer et al. 2016) as well as with the publicly available LVK 3D skymap. We also interpolate the posterior distribution with a Gaussian process (GP) density estimator (D'Emilio et al. 2021), which comes with an associated

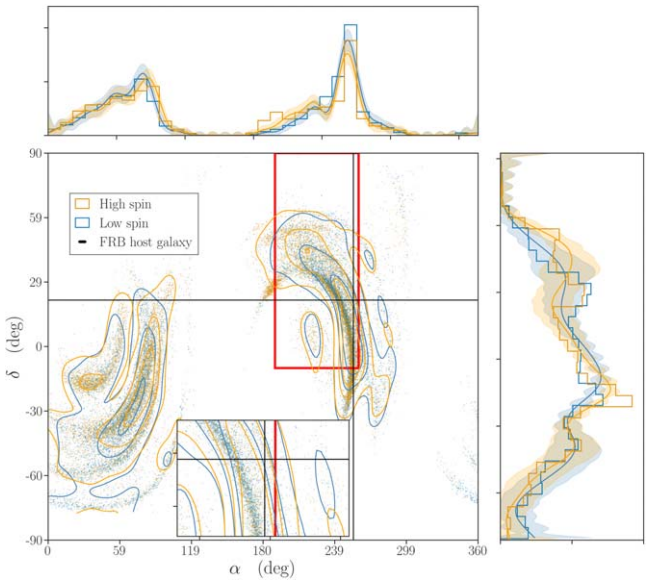

Figure 2. Skymap for GW190425 event, obtained both with high-spin and low-spin priors. The red box shows CHIME's instantaneous FOV at the time of GW190425. Interpolation was generated with a two-dimensional GP density estimator (contour lines). The location of FRB20190425A's most probable host galaxy (UGC10667) is annotated for comparison.

fit uncertainty. As best illustrated by Figure 1, we believe the public 3D skymap interpolation to be inaccurate in three dimensions since important density features are smoothed out. Hence, we only report results obtained with the ClusteredKDE and the GP density estimates.

To better understand the individual contributions of the joint integral, we also calculate the odds association by approximating $\mathcal{I}_{D_L,\Omega} \approx \mathcal{I}_{D_L}\mathcal{I}_{\Omega}$. Since the $\mathcal{I}_{D_L}$ integral is in one-dimension, it is computed with a Gaussian KDE; while the two-dimensional $\mathcal{I}_{\Omega}$ is computed with the `ligo.skymap` package. We also compute both integral interpolations with a GP density estimator, for comparison. The latter are shown in Figure 2.

2.2. Instantaneous Field-of-view of CHIME

In Earth-fixed coordinates, CHIME looks directly over LIGO Hanford and near the region of the largest antenna response. Moreover, the LIGO-Virgo detector network preferentially detects signals from directly overhead/underneath. Due to this, FRBs observed within a few hours of a GW trigger will have a higher probability of chance sky position overlap than FRBs observed at other times.

Therefore, we need to account for this non-negligible correlation between CHIME and the LIGO detectors due to CHIME's instantaneous field of view (FOV). We encode the correlations between the two instruments entirely in the spatial overlap prior, i.e., the denominator of Equation (1), such that it corresponds to their common FOV viewing window. We modify the default full sky prior $\pi(\Omega|\text{Full Sky})$, from Romero-Shaw et al. (2020) by assuming an overlapping time coincidence window of $[-2, 2.5]$ hr.[5]

The instantaneous FOV of CHIME at the time of the event, centered around our choice of the overlapping time coincidence window, defines $\pi(\Omega|\text{FOV})$. This is shown as the red box in Figure 2. It effectively restricts the full sky prior and hence we expect to reduce the chances for coincidence by about a factor of 5. The limited sky prior coincides with a large region of the GW190425's skymap, where we have used a GP estimator to interpolate the LVK public samples. We also note that the location of the presumed host galaxy falls just about within the 50% probability contours of the GP density estimator, as shown by black crossing lines.

The posterior overlap integral results are shown in Table 1 for both low-spin and high-spin samples and for both spatial priors $\pi(\Omega|\text{FOV})$ and $\pi(\Omega|\text{Full Sky})$. We note that the latter are only included for comparison since we do believe that the full sky prior causes an overestimate of the association odds in the case of CHIME-detected counterparts. The GP's high-spin results are consistent, within their uncertainty, with the values obtained with KDEs. The GP's low-spin results present a larger discrepancy with the KDEs, in some cases. We blame this on the posterior surface of low-spin results being narrower and therefore the FRB location lying right on the edge of the 50% spatial overlap probability contours. We also note that for the approximately disjoint integral $\mathcal{I}_{D_L}\mathcal{I}_{\Omega}$, most of the support is given by correlations with the luminosity distance, which increases the overall integral value. We conclude the values obtained with the high-spin prior samples, which allow for the spinning HMNS hypothesis, are the most trustworthy, and hence we take $\mathcal{I}_{D_L,\Omega} \approx 10$.

2.3. Temporal Overlap and Prior Odds

Following Ashton et al. (2018), we can write the temporal overlap integral for the time of coalescence t_c for GW190425 and FRB20190425A as

$$\mathcal{I}_{t_c} = \begin{cases} \frac{T}{\Delta t} & \text{if } (t_c - t_{\rm EM}) \in [\Delta t^{\rm min}, \Delta t^{\rm max}] \\ 0 & \text{otherwise} \end{cases}, \tag{3}$$

where Δt is defined as the window used to search for GW and FRB coincident events and where T is the total co-observation time for both transient surveys. Now, the prior odds can be written in terms of the GW, EM, and joint detection rates as

$$\pi_{C/R} \approx \frac{R_{\rm GW,EM}}{R_{\rm GW} R_{\rm EM} T}. \tag{4}$$

We have little information on the rates of BNS detections with or without FRB counterparts, specifically, FRB signals detectable by CHIME. For the special case in which we are in $R_{\rm GW} \approx R_{\rm GW,EM} \ll R_{\rm EM}$, hence we must thus have

$$\pi_{C/R} \approx \frac{1}{R_{\rm EM} T}. \tag{5}$$

2.4. Posterior Odds

We can now write the posterior odds between the coincident hypothesis C and the random association R by combining the spatial and temporal overlap integrals with the prior odds $\pi_{C/R}$. This choice leads to the posterior odds not to explicitly depend on the co-observation time T, we can therefore write the odds as

$$\mathcal{O}_{C/R} \approx \frac{1}{R_{\rm EM} \Delta t} \mathcal{I}_{D_L,\Omega}. \tag{6}$$

We proceed to estimate $R_{\rm EM}$ by using the observed CHIME FRB detection rate using the latest catalog release (Amiri et al. 2021). Using the 536 FRBs observed in 341 days, we estimate

[5] The requirement for coincidence is a window of $[-2, 24]$ hr in Moroianu et al. (2023).

Table 1
Spatial Overlap Probabilities and Constituent Elements for Two Spin Priors, Calculated Assuming Planck 2015 Cosmology and Using GWTC-3 Samples

Prior Assumptions		$\mathcal{I}_{D_L,\Omega}$		$\mathcal{I}_{D_L}\mathcal{I}_{\Omega}$		$\mathcal{I}_{D_L}$		$\mathcal{I}_{\Omega}$	
		KDE	GP	KDE	GP	KDE	GP	KDE	GP
Low-spin	$\pi(\Omega\|\text{Full Sky})$	45.7	$72.5^{+4.6}_{-4.6}$	9.2	81.1^{+40}_{-40}	12.4	$12.7^{+6.1}_{-6.1}$	0.7	$6.4^{+0.8}_{-0.8}$
	$\pi(\Omega\|\text{FOV})$	8.9	$14.1^{+0.9}_{-0.9}$	1.8	$15.7^{+7.9}_{-7.9}$	⋯	⋯	0.1	$1.2^{+0.1}_{-0.1}$
High-spin	$\pi(\Omega\|\text{Full Sky})$	52.1	$50.3^{+3.8}_{-3.8}$	52.1	63.8^{+30}_{-30}	13.4	$13.5^{+6.1}_{-6.1}$	3.8	$4.7^{+0.8}_{-0.8}$
	$\pi(\Omega\|\text{FOV})$	10.1	$9.8^{+0.7}_{-0.7}$	10.1	$12.4^{+5.0}_{-5.0}$	⋯	⋯	0.7	$0.9^{+0.1}_{-0.1}$

Note. We report values obtained with two KDE methods (public LIGO `FITS` file for $\mathcal{I}_{\Omega}$ and `LIGO.skymap`'s ClusteredKDE for $\mathcal{I}_{D_L,\Omega}$) and a GP density estimator.

$R_{\rm CHIME} \approx 1.6\,{\rm day}^{-1}$, where we have made the simplifying assumption that the CHIME instrument had zero downtime.

The analysis performed in Moroianu et al. (2023) used a search window around O3a GW triggers of $\Delta t \approx 26$ hr (2 hr in the past and 24 hr in the future). Using the same search window, we obtain $(R_{\rm EM}\Delta t)^{-1} \approx 0.5$. Consequently, the posterior odds are $\mathcal{O}_{C/R} \approx 5$ assuming high-spin spin prior.

We can compute an optimistic estimate for the posterior odds by using a search window of $\Delta t \approx 3$ hr (corresponding roughly to the time delay between GW190425 and FRB20190425A), obtaining $(R_{\rm EM}\Delta t)^{-1} \approx 5$ and thus the corresponding posterior odds are $\mathcal{O}_{C/R} \approx 50$. Our full results are summarized in Table 2. We positively highlight the sensitivity of our calculations to our prior assumptions, suggesting the importance of careful consideration of the latter. Our optimistic ($\Delta t \approx 3$ hr) versus agnostic ($\Delta t \approx 26$ hr) priors on the time window result in about $\mathcal{O}(10)$ discrepancy in the odds. Similarly, the discrepancy in results between un-informed (full-sky prior $\pi(\Omega|\text{Full Sky})$) and informed (spatial overlap $\pi(\Omega|\text{FOV})$) priors is about $\mathcal{O}(5)$.

We note that we have included all 62 bursts from repeating sources in Amiri et al. (2021) in our estimates to best estimate CHIME's detection sensitivity. Not including these would reduce our FRB event count to 474 bursts. Therefore, our estimate for the CHIME detection rate would be $R_{\rm CHIME} \approx 1.4\,{\rm day}^{-1}$. Consequently, all the posterior odds reported in this work would increase by around 14%.

Table 2
Posterior Odds $\mathcal{O}_{C/R}$ Calculated Using the Overlap Integral $\mathcal{I}_{D_L,\Omega}$ for Two Values for Δt: the Actual Search Window Used by Moroianu et al. (2023) and the Approximate Time Delay between Transients

Prior Assumptions		$\Delta t \approx 26$ hr		$\Delta t \approx 3$ hr	
		KDE	GP	KDE	GP
Low-spin	$\pi(\Omega\|\text{Full Sky})$	22.8	$36.2^{+2.3}_{-2.3}$	228	362^{+23}_{-23}
	$\pi(\Omega\|\text{FOV})$	4.5	$7.0^{+1.1}_{-1.1}$	44.5	$70.5^{+4.5}_{-4.5}$
High-spin	$\pi(\Omega\|\text{Full Sky})$	26.0	$25.1^{+1.9}_{-1.9}$	260	251^{+19}_{-19}
	$\pi(\Omega\|\text{FOV})$	5.0	$4.9^{+0.3}_{-0.3}$	50.5	$49^{+3.5}_{-3.5}$

3. GW190425 Parameter Estimation with UGC10667 as Its Host Galaxy

We perform Bayesian parameter estimation with `BILBY` (Ashton et al. 2019; Romero-Shaw et al. 2020) using the `DYNESTY` nested sampling library (Speagle 2020). We use the publicly available strain data for GW190425 (LVK Scientific Collaboration 2020b) observed by both the LIGO Hanford and Virgo detectors. To reduce the computational costs, the analysis is performed using the reduced order quadrature approximation (Smith et al. 2016; Baylor et al. 2019), using the GW waveform model `IMRPhenomPv2_NRTidal` (Dietrich et al. 2017, 2019), which includes both tidal and precession effects as in Abbott et al. (2024). We closely follow the analysis configuration performed in Abbott et al. (2024), namely we maintain the same prior probability distributions on the GW binary parameters, such that we produce two sets of results: low-spin and high-spin priors. These correspond to dimensionless spin magnitudes for both components to be within the ranges $\chi_{1,2} < 0.05$ and $\chi_{1,2} < 0.89$, respectively.

To investigate the effects on the GW190425 parameter estimation results when we assume that UGC10667 was indeed the true host galaxy, we impose two distinct, and progressively stricter, constraints: we fix the sky location to $(\alpha, \delta) = (255.^{\circ}72, 21.^{\circ}52)$, the sky location of UGC10667 (Moroianu et al. 2023), and then we also fix the GW luminosity distance to the one of UGC10667, corresponding to the spectroscopic redshift estimate for UGC10667 of $z = 0.03136 \pm 0.00009$ (Abazajian et al. 2009), such that the galaxy position is fixed.

In Figure 3, we show the inferred posterior distributions on the total mass $m_{\rm tot}$, the mass ratio q, and the effective inspiral spin parameter $\chi_{\rm eff}$ for GW190425 under both low-spin and high-spin assumptions and with both the fixed sky and fixed position configurations. Similarly, in Figure 4, we show the marginalized posterior distributions on the primary m_1 and the secondary m_2 masses (both in the source frame) for GW190425. Lastly, the posterior distributions on the luminosity distance D_L and the inclination angle ι are shown in Figure 5. For all results, we show the GW190425 posterior distribution inferred by the LVK (Abbott et al. 2020a) for reference.

For the low-spin prior we find that the total mass and mass ratio are consistent with the LVK results for the fixed sky case, namely we find that the mass ratio must be greater than $q = 0.7$ at 68% confidence and the total mass is $3.30^{+0.06}_{-0.04}\,M_{\odot}$. Meanwhile, when we fix the redshift to that of the UGC10667 galaxy position, the fixed position case only allows total masses greater than $m_{\rm tot} = 3.3 M_{\odot}$ at 99.9% confidence, namely we find $3.32^{+0.04}_{-0.01}\,M_{\odot}$. For all runs, we find consistent posteriors on $\chi_{\rm eff}$.

For the high-spin prior we find consistent results for all intrinsic parameters. However, the mass ratio posteriors are bimodal allowing for mass ratios around $q = 0.45$ and we can constrain q to be as low as $q = 0.3$ with 99% confidence. The total mass in this case is allowed to be higher than in the LVK case, due to the increased spin support (see Table 3 for explicit values). As for $\chi_{\rm eff}$, we find that $\chi_{\rm eff} > 0$ at 99% confidence, meaning that the binary can be highly spinning with positively aligned spins.

We find that fixing the sky location constrains the luminosity distance and inclination to approximately the same distribution for both spin prior assumptions, as shown in Figure 5. This effect can be understood as coming from the antenna pattern

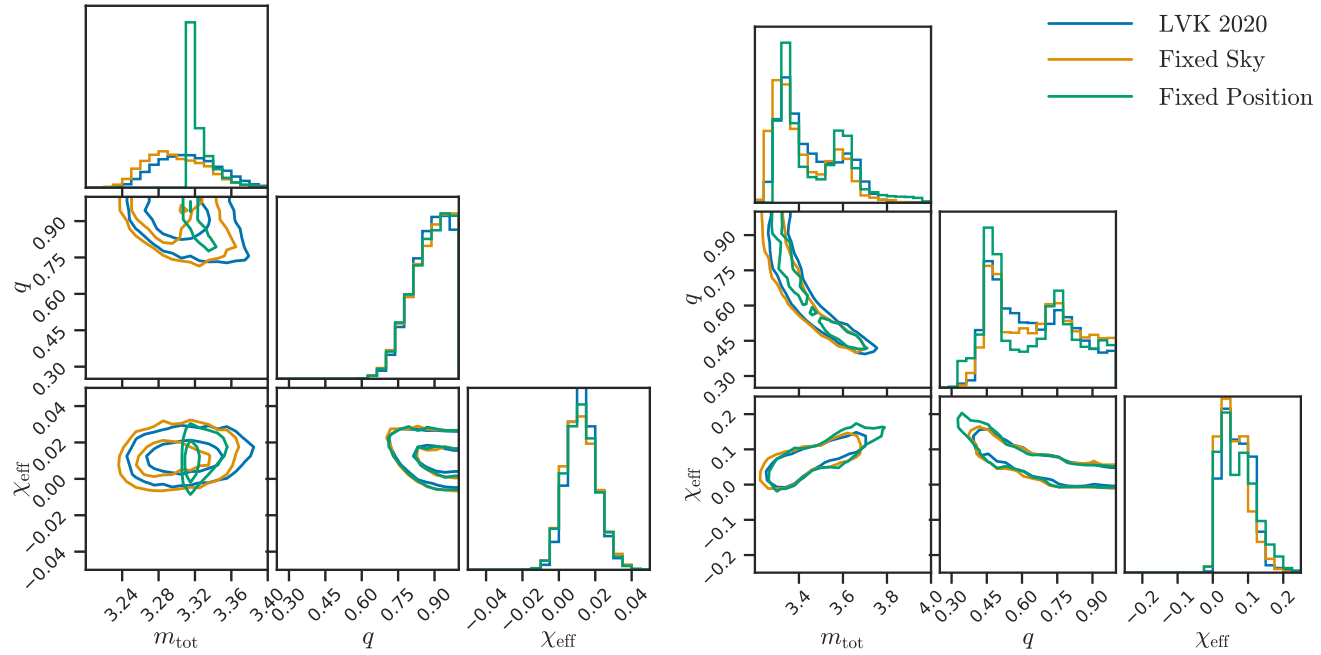

Figure 3. Corner plot showing the marginalized posterior distributions on the total mass $m_{\rm tot}$, the mass ratio q, and the effective inspiral spin parameter $\chi_{\rm eff}$ for GW190425 for both the low-spin (left panel) and high-spin (right panel) priors under the fixed sky location (orange) and fixed position (green) assumptions as described in Section 3. For both cases, we also show the corresponding results from Abbott et al. (2020a) for reference (blue).

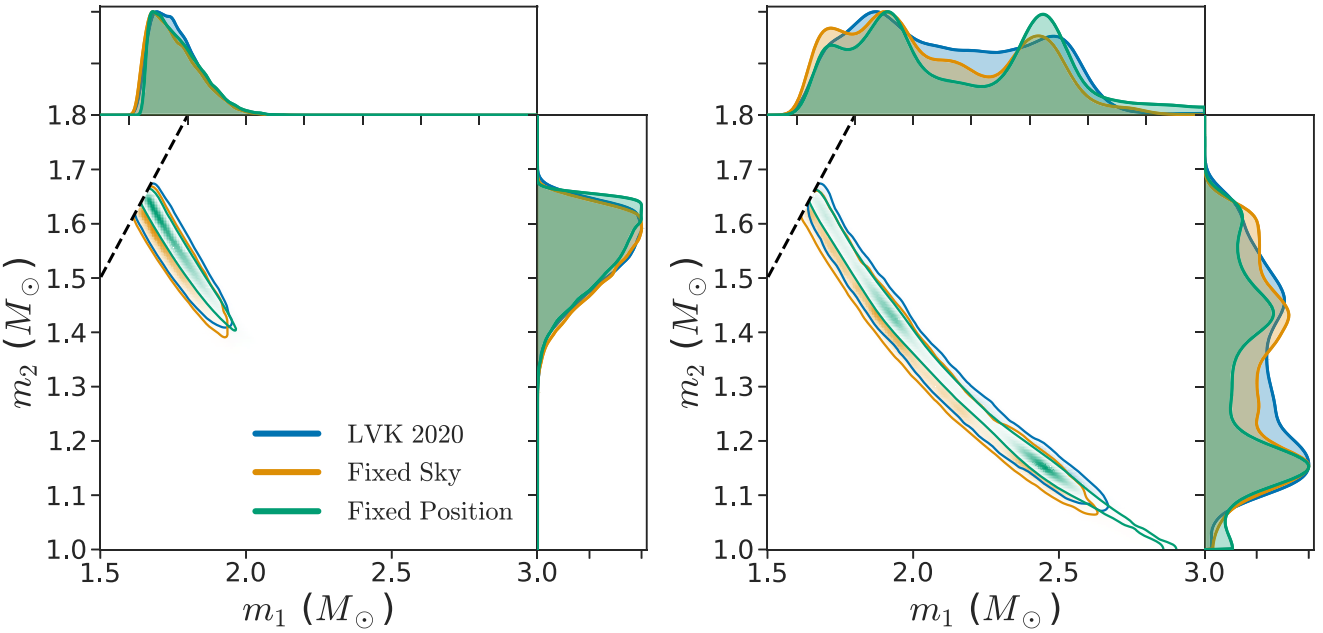

Figure 4. Marginalized posterior distributions on the primary mass m_1 and the secondary mass m_2 (both in the source frame) for GW190425 for both the low-spin (left panel) and high-spin (right panel) priors under the fixed sky location (orange) and fixed position (green) assumptions as described in Section 3. For both cases, we also show the primary and secondary mass posteriors from Abbott et al. (2020a) for reference (blue).

response functions, which depend on the sky location, constraining how the GW signal power is divided between both GW polarization amplitudes.

Since the luminosity distance and inclination angle degeneracy are broken for all the assumptions considered in this work, it is useful to show the marginalized posterior distribution for the viewing angle θ_c (shown in Figure 6) to more clearly show that under the assumption that UGC10667 was indeed the host galaxy of GW190425 then it must have been an off-axis merger and consequently lead to effects on the expected EM emission (Bhardwaj et al. 2023a).

Finally, we provide a summary of the measured GW190425 parameters under the assumptions described in this section. The summary includes both the low-spin and high-spin prior results, with both the fixed sky and fixed position assumptions in Table 3.

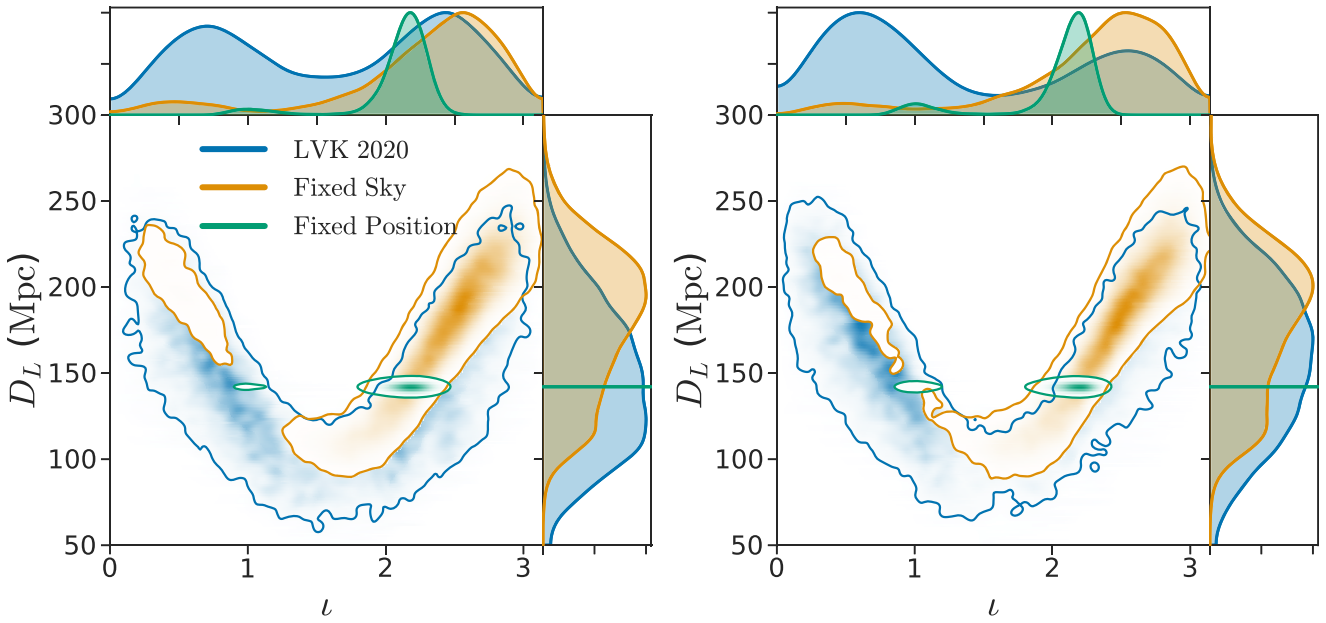

Figure 5. Marginalized posterior distributions on the luminosity distance D_L and the inclination angle ι for GW190425 for both the low-spin (left panel) and high-spin (right panel) priors under the fixed sky location (orange) and fixed position (green) assumptions as described in Section 3. For both cases, we also show the results from Abbott et al. (2020a) for reference (blue).

Table 3
Summary of Updated Parameters for GW190425 Using Both the Low-spin and High-spin Priors under the Fixed Sky and Fixed Position Assumptions as Described in Section 3

	Low-spin Prior		High-spin Prior	
	Fixed Sky	Fixed Position	Fixed Sky	Fixed Position
Primary mass $m_1/M_\odot$	$1.74^{+0.17}_{-0.09}$	$1.75^{+0.17}_{-0.09}$	$2.01^{+0.53}_{-0.33}$	$2.10^{+0.59}_{-0.40}$
Secondary mass $m_2/M_\odot$	$1.55^{+0.08}_{-0.14}$	$1.57^{+0.08}_{-0.13}$	$1.35^{+0.26}_{-0.25}$	$1.32^{+0.30}_{-0.26}$
Chirp mass $\mathcal{M}/M_\odot$	$1.43^{+0.02}_{-0.02}$	$1.442^{+0.001}_{-0.001}$	$1.43^{+0.02}_{-0.02}$	$1.442^{+0.001}_{-0.001}$
Mass ratio m_2/m_1	$0.89^{+0.10}_{-0.15}$	$0.89^{+0.10}_{-0.15}$	$0.67^{+0.29}_{-0.24}$	$0.63^{+0.32}_{-0.24}$
Total mass $m_{\rm tot}/M_\odot$	$3.30^{+0.06}_{-0.04}$	$3.32^{+0.04}_{-0.01}$	$3.37^{+0.28}_{-0.11}$	$3.42^{+0.34}_{-0.11}$
Effective inspiral spin parameter $\chi_{\rm eff}$	$0.01^{+0.02}_{-0.01}$	$0.01^{+0.02}_{-0.01}$	$0.06^{+0.08}_{-0.05}$	$0.07^{+0.10}_{-0.06}$
Luminosity distance $D_{\rm L}$	$183.7^{+58.2}_{-75.3}$ Mpc	…	$183.2^{+57.8}_{-73.3}$ Mpc	…
Viewing angle θ_v	$37.8^{+42.4}_{-27.5}$ deg	$56.1^{+14.3}_{-9.7}$ deg	$37.8^{+41.3}_{-26.9}$ deg	$55.6^{+14.3}_{-9.2}$ deg

Note. We report all mass measurements in the source frame assuming a Planck 2015 cosmological model.

3.1. Probability of Prompt Collapse

High-mass mergers such as GW190425 are expected to promptly produce a black hole, resulting in a small amount of ejecta, that are especially rich in lanthanides. This scenario likely results in a faint, particularly red EM counterpart (Foley et al. 2020), hence explaining the lack of KN detection. To check this possibility, we repeat the analysis of Abbott et al. (2020a) and compute the probability of prompt collapse as well as the threshold mass $M_{\rm threshold}$ for which BNS systems are expected to collapse into a black hole promptly after merger. To estimate the threshold mass, as in Abbott et al. (2020a), we consider two cases: (1) using EOS constraints from GW170817 and (2) additionally imposing a maximum Tolman–Oppenheimer–Volkoff (TOV) limit mass $M_{\rm TOV}^{\rm max} \geqslant 1.97 M_\odot$. We use the estimated maximum mass for GW190425 with the fixed position posterior samples to estimate the mass of the resulting NS after the merger. First, we note that this updated total mass estimate is still $>3.2 M_\odot$ for all priors considered in this study, therefore still supporting a high mass merger, as in Abbott et al. (2020a). In Figure 7, we show the posterior distribution for the total mass of GW190425 compared to the inferred $M_{\rm threshold}$. Following Agathos et al. (2020), the prompt collapse probability can be calculated as

$$P(\mathrm{PC}_{\rm GW190425}|d) = P(m_{\rm tot} > M_{\rm threshold}) = P(m_{\rm tot} - M_{\rm threshold} > 0), \quad (7)$$

where d is the GW observed data. We find that since the total mass for GW190425 increases when fixing the position of its host to UGC10667, the corresponding probabilities for prompt collapse are above 88% for all spin priors. Specifically for high-spin priors, we find 98% when assuming EOS constraints from GW170817 only and 94% by additionally imposing a maximum TOV mass constraint.

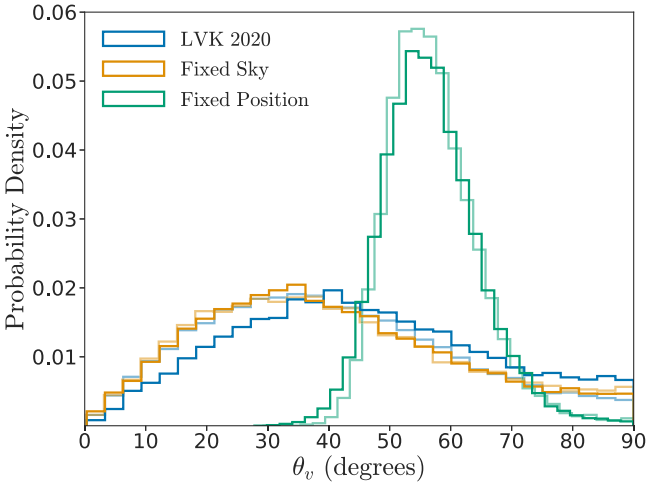

Figure 6. Marginalized posterior distributions on the viewing angle θ_v for GW190425 under the fixed sky location (orange) and fixed position assumptions (green) as described in Section 3. For both cases, we also show the viewing angle posteriors computed using the results of Abbott et al. (2020a) for reference (blue). We show both the low-spin (light lines) and high-spin (solid lines) prior results for completeness.

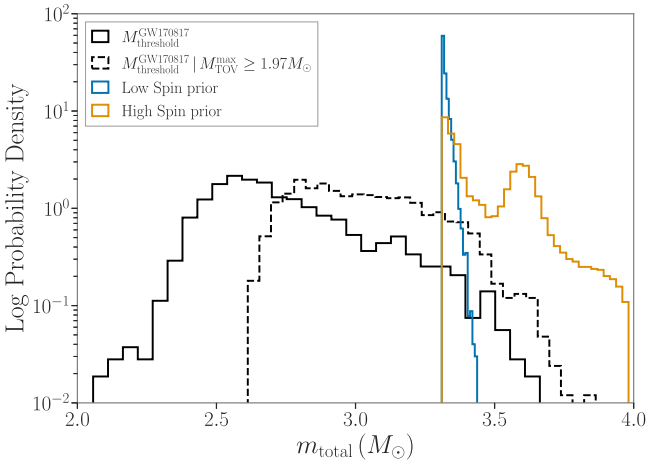

Figure 7. Posterior distributions on the total mass $m_{\rm tot}$ for GW190425 from the fixed 3D sky position of UGC10667 parameter estimation results for both low (blue) and high spin (yellow) priors. We also show the estimated prompt collapse threshold mass $M_{\rm threshold}$ posteriors, conditional on EOS constraints from GW170817 (solid black) and with the additional constraint assuming $M_{\rm TOV}^{\rm max} \geqslant 1.97 M_\odot$ (dashed black).

4. Conclusion

In this work, we have investigated the association between the GW event GW190425 and its presumed EM counterpart FRB20190425A. We have recalculated the probability of association as a Bayesian hypothesis comparing the hypothesis between a common source for the transients and the chance of a random source association. The posterior odds were calculated, following previous work, as a product of temporal and spatial overlap integrals. We found that the spatial overlap can marginally support a common source hypothesis, yielding a value of $\mathcal{O}(50)$. However, since both the CHIME observatory and the LIGO interferometers point in similar directions, the significance of the spatial overlap is lowered to $\mathcal{O}(10)$. The temporal overlap integrals yield less favorable results since they take into account the correlations between the instruments. The overall posterior odds were found to be $\mathcal{O}(5)$ and to only minimally support the association claimed by Moroianu et al. (2023).

We further investigate the association by rerunning parameter estimation with the sky location of UGC10667, the host galaxy for the FRB20190425A counterpart identified by Bhardwaj et al. (2023b), as well as with its measured redshift. The end-to-end parameter estimation analysis for the claimed associated transients is shown in this work in its entirety. Some of these, such as the viewing angle results, have been used by Bhardwaj et al. (2023a) to argue against the association hypothesis.

To conclude, we bring forward a word of caution when performing GW and EM counterpart associations, as shown in this work, simple spatial and temporal coincidences are useful and can in principle rule out potential associations (see Ashton et al. 2018); however, for the case considered, more observations of potentially associated GW and FRB counterparts will be needed to potentially shed light on the possibility of such transients having a common origin.

Acknowledgments

The authors would like to thank David Kaplan, Jolien Creighton and Patrick Brady for their useful comments and feedback throughout this work. I.M.H. is supported by a McWilliams postdoctoral fellowship at Carnegie Mellon University. I.M.H. acknowledges support from NSF Award Nos. PHY-1912649 and PHY-2207728. V.D.E. is supported by NSF's LIGO Laboratory, which is a major facility fully funded by the National Science Foundation, operating under cooperative agreements PHY-1764464 and PHY-2309200. Additional support comes from NSF Award 2207758. The authors are grateful for computational resources provided by the Leonard E Parker Center for Gravitation, Cosmology and Astrophysics at the University of Wisconsin-Milwaukee and supported by NSF awards PHY-1912649, as well as computational resources provided by Cardiff University and supported by STFC grant ST/V001337/1 (UK LIGO Operations award). We thank LIGO and Virgo Collaboration for providing the data for this work. This research has made use of data, software, and/or web tools obtained from the Gravitational Wave Open Science Center (https://www.gw-openscience.org/), a service of LIGO Laboratory, the LIGO Scientific Collaboration and the Virgo Collaboration. LIGO Laboratory and Advanced LIGO are funded by the United States National Science Foundation (NSF) as well as the Science and Technology Facilities Council (STFC) of the United Kingdom, the Max-Planck-Society (MPS), and the State of Niedersachsen/Germany for support of the construction of Advanced LIGO and construction and operation of the GEO600 detector. Additional support for Advanced LIGO was provided by the Australian Research Council. Virgo is funded, through the European Gravitational Observatory (EGO), by the French Centre National de Recherche Scientifique (CNRS), the Italian Istituto Nazionale di Fisica Nucleare (INFN), and the Dutch Nikhef, with contributions by institutions from Belgium, Germany, Greece, Hungary, Ireland, Japan, Monaco, Poland, Portugal, Spain. This material is based upon work supported by NSF's LIGO Laboratory, which is a major facility fully funded by the National Science Foundation. This Letter has been assigned LIGO document number LIGO-P2400106.

ORCID iDs

Ignacio Magaña Hernandez https://orcid.org/0000-0003-2362-0459
Virginia d'Emilio https://orcid.org/0000-0001-6145-8187
Soichiro Morisaki https://orcid.org/0000-0002-8445-6747
Mohit Bhardwaj https://orcid.org/0000-0002-3615-3514
Antonella Palmese https://orcid.org/0000-0002-6011-0530

References

Aasi, J., Abbott, B., Abbott, R., et al. 2015, CQGra, 32, 074001
Abazajian, K. N., Adelman-McCarthy, J., Agüeros, M., et al. 2009, ApJS, 182, 543
Abbott, B. P., Abbott, R., Abbott, T., et al. 2019, PhRvX, 9, 011001
Abbott, B. P., Abbott, R., Abbott, T., et al. 2020a, ApJ, 892, L3
Abbott, B. P., Abbott, R., Abbott, T., et al. 2017, ApJL, 848, L13
Abbott, B. P., Abbott, R., Abbott, T., et al. 2020b, ApJL, 892, L3
Abbott, R., Abbott, T. D., T. D., Acernese, et al. 2024, PhRvD, 109, 022001
Abbott, R., Abbott, T. D., Acernese, F., et al. 2023, PhRvX, 13, 041039
Acernese, F. A., Agathos, M., Agatsuma, K., et al. 2014, CQGra, 32, 024001
Agathos, M., Zappa, F., Bernuzzi, S., et al. 2020, PhRvD, 101, 044006
Akutsu, T., Ando, M., Arai, K., et al. 2021, PTEP, 2021, 05A101
Amiri, M., Andersen, B., Bandura, K., et al. 2021, ApJS, 257, 59
Ashton, G., Ackley, K., Magaña Hernandez, I., & Piotrzkowski, B. 2021, CQGra, 38, 235004
Ashton, G., Burns, E., Dal Canton, T., et al. 2018, ApJ, 860, 6
Ashton, G., Hübner, M., Lasky, P. D., et al. 2019, ApJS, 241, 27
Balasubramanian, A., Corsi, A., Mooley, K. P., et al. 2022, ApJ, 938, 12
Baylor, A., Smith, R., & Chase, E. 2019, IMRPhenomPv2_NRTidal_GW190425_narrow_Mc, v1, Zenodo, doi:10.5281/zenodo.3478659
Bhardwaj, M., Palmese, A., Magaña Hernandez, I., D'Emilio, V., & Morisaki, S. 2023a, arXiv:2306.00948
Bhardwaj, M., Michilli, D., Kirichenko, A. Y., et al. 2023b, arXiv:2310.10018
Dietrich, T., Bernuzzi, S., & Tichy, W. 2017, PhRvD, 96, 121501
Dietrich, T., Khan, S., Dudi, R., et al. 2019, PhRvD, 99, 024029
D'Emilio, V., Green, R., & Raymond, V. 2021, MNRAS, 508, 2090
Foley, R. J., Coulter, D. A., Kilpatrick, C. D., et al. 2020, MNRAS, 494, 190
LVK Scientific Collaboration 2020a, Parameter estimation sample release for GW190425, LIGO Document P2000026-v2, https://dcc.ligo.org/LIGO-P2000026/public
LVK Scientific Collaboration 2020b, GW190425, O3_Discovery_Papers, doi:10.7935/ggb8-1v94
Moroianu, A., Wen, L., James, C. W., et al. 2023, NatAs, 7, 579
Nicholl, M., Berger, E., Kasen, D., et al. 2017, ApJ, 848, L18
Panther, F. H., Anderson, G. E., Bhandari, S., et al. 2023, MNRAS, 519, 2235
Piotrzkowski, B., Baylor, A., & Magaña Hernandez, I. 2022, CQGra, 39, 085010
Romero-Shaw, I. M., Talbot, C., Biscoveanu, S., et al. 2020, MNRAS, 499, 3295
Singer, L. P., Chen, H.-Y., Holz, D. E., et al. 2016, ApJL, 829, L15
Smartt, S., Nicholl, M., Srivastav, S., et al. 2024, MNRAS, 528, 2299
Smith, R., Field, S. E., Blackburn, K., et al. 2016, PhRvD, 94, 044031
Soares-Santos, M., Holz, D., Annis, J., et al. 2017, ApJL, 848, L16
Speagle, J. S. 2020, MNRAS, 493, 3132
Zhang, B. 2023, RvMP, 95, 035005